Realization of In-Plane p–n Junctions with Continuous Lattice of a Homogeneous Material

Xiaochun Huang, Bing Liu, Jiaqi Guan, Guangyao Miao, Zijian Lin, Qichang An, Xuetao Zhu, Weihua Wang, and Jiandong Guo*

Two-dimensional (2D) in-plane p–n junctions with a continuous interface have great potential in next-generation devices. To date, the general fabrication strategies rely on lateral epitaxial growth of p- and n-type 2D semiconductors. An in-plane p–n junction is fabricated with homogeneous monolayer Te at the step edge on graphene/6H-SiC(0001). Scanning tunneling spectroscopy reveals that Te on the terrace of trilayer graphene is p-type, and it is n-type on monolayer graphene. Atomic-resolution images demonstrate the continuous lattice of the junction, and mappings of the electronic states visualize the type-II band bending across the space-charge region of 6.2 nm with a build-in field of 4×10^5 V cm^{-1}. The reported strategy can be extended to other 2D semiconductors on patternable substrates for designed fabrication of in-plane junctions.

The flourish of two-dimensional (2D) atomic crystals[1–8] and the advances in van der Waals epitaxial growth technology[9–16] stimulate tremendous interest in the fabrication of 2D in-plane p–n junctions, which have great potential in the next-generation integrated circuits and optoelectronic devices.[15,17–21] To date, the fabrication strategies rely on the lateral epitaxial growth of p- and n-type 2D semiconductors. Based on transition metal dichalcogenides, the lateral epitaxial growth has been realized in systems such as MoS_2–WS_2 and WSe_2–MoS_2.[15,19] However, at these heterointerfaces, chemical intermixing may occur such that lattice disorder is inevitable. Besides, the lattice mismatch also induces interfacial scattering, and thus deteriorates the device performance.[22]

Dr. X. C. Huang, Dr. B. Liu, Dr. J. Q. Guan, Dr. G. Y. Miao, Dr. Z. J. Lin,
Dr. Q. C. An, Prof. X. Zhu, Prof. W. Wang, Prof. J. Guo
Beijing National Laboratory for Condensed Matter Physics &
Institute of Physics
Chinese Academy of Sciences
Beijing 100190, China
E-mail: jdguo@iphy.ac.cn
Dr. X. C. Huang, Dr. B. Liu, Dr. J. Q. Guan, Dr. G. Y. Miao, Dr. Z. J. Lin,
Dr. Q. C. An, Prof. X. Zhu, Prof. J. Guo
School of Physical Sciences
University of Chinese Academy of Sciences
Beijing 100049, China
Prof. J. Guo
Collaborative Innovation Center of Quantum Matter
Beijing 100871, China

The ORCID identification number(s) for the author(s) of this article can be found under https://doi.org/10.1002/adma.201802065.

An in-plane p–n junction with continuous lattice by a homogeneous material would be particularly ideal for applications. The experimental realization relies on: 1) a prepatterned substrate that can modulate, with spatial variance, the electronic band structures of the overlayer; 2) an ultrathin semiconductor film with continuous lattice across the pattern edge of the underlying template; and 3) the carrier type of the semiconductor film can be inverted by the template tuning. In this study, we choose 6H-SiC(0001) (referred to as SiC in the following) as the substrate. With proper treatment, the surface is covered by few-layer graphene whose thickness can be controlled. The graphene/SiC normally dopes electrons to the epitaxial films, and the doping level can be modulated by the graphene thickness[23–27] (see **Figure 1**a). The recently synthesized monolayer (ML) Te is chosen as the semiconductor film.[4] We obtain ML Te films in p-type grown on trilayer (TL) graphene/SiC, and in n-type on bilayer (BL) or ML graphene/SiC. Furthermore, we epitaxially grow an ML Te film covering the ML and TL graphene/SiC terraces with continuous lattice across the step edge, and realize a 2D in-plane p–n junction by one single homogeneous material. As characterized by in situ scanning tunneling microscopy/spectroscopy (STM/STS), the type-II band alignment with a narrow space charge region of ≈6.2 nm and a large build-in field of 4×10^5 V cm^{-1} are observed at the junction.

Adopting the standard graphitization process with the annealing conditions carefully optimized,[25,28] we obtain SiC substrate covered by graphene with different number of atomic layers in a controlled way (the details of the annealing process are described in the Supporting Information). The thickness of graphene can be identified based on the characteristics of STM images and the location of Dirac point measured by the dI/dV spectra.[29] Monolayer Te is grown on graphene/SiC substrate by molecular beam epitaxy.[4] The film is composed of parallel-arranged helical chains (Figure 1b), which can spread across different graphene terraces with continuous lattice at the step edges. In the current work, we grow Te films at the substrate temperature of 100 °C to enhance the formation of monolayer films. Monolayer Te nanoribbons with the width ranging from 8 to 23 nm are observed (without width dependence of the electronic structures, see the Supporting Information for detail).

Figure 2a shows the STM image of ML Te on TL graphene/SiC. The thickness of the underlying graphene can be identified
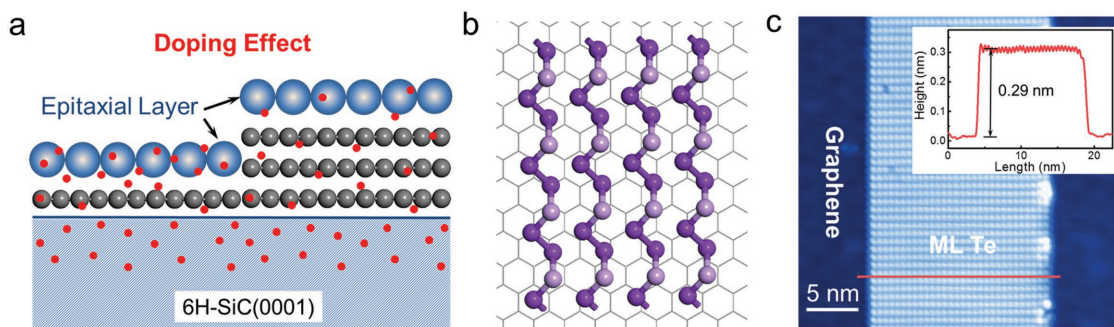
Figure 1. Electron doping effect of graphene/SiC substrate and the morphology of ML Te on graphene/SiC. a) Schematic diagram of a monolayer epitaxial film (blue balls) grown on ML and TL graphene (gray balls) on SiC. The SiC substrate acts as a reservoir of electrons (red dots), which induces the n-type doping to graphene and even the epitaxial film. On the other hand, the graphene layer screens the n-type doping—the thicker the graphene is, the weaker the doping to the epitaxial film. b) Schematic drawing of ML Te film on graphene. The Te helical chains are flat lying on graphene in parallel. The topmost Te atoms in each chain are highlighted in pink, which presents the rectangular lattice observed by STM. c) High-resolution STM image (-2.0 V/20 pA) of an ML Te nanoribbon on graphene/SiC. The height profile along the red line is shown in the inset.

by the location of Dirac point (≈ -0.20 V, see Figure 2j).[29] The dI/dV spectra measured along the red dashed line are plotted in a color-coded map in Figure 2d, indicating the homogeneous electronic bands of the Te film, i.e., the identical positions of the valence band maximum (E_V) and conduction band minimum (E_C) at different sites within the film, respectively. The position of Fermi level (E_F) at zero bias is closer to E_V than E_C, revealing the p-type characteristic. The quantitative information is clearly shown in Figure 2g, i.e., E_V at -0.43 eV and E_C at 0.66 eV. The band gap E_g is determined as $E_C - E_V = 1.09$ eV, while the center between E_C and E_V, i.e., $E_i = (E_C + E_V)/2$ is located at $+0.12$ eV. Note that the sign of E_i reflects the carrier type, i.e., the positive corresponds to p-type, while the negative corresponds to n-type as shown in the following.

On the ML Te grown on BL graphene/SiC (the Dirac point is located at -0.34 V as shown in Figure 2j), E_V is dramatically lowered to -0.70 eV and E_C to 0.35 eV, resulting in the change of E_i to -0.18 eV (Figure 2e,h). This is the signature of an n-type semiconductor, i.e., the carrier type of Te is reversed due to the doping effect of the graphene/SiC. Similar results are obtained on ML Te grown on ML graphene/SiC (Figure 2c,f,i). The values of E_C, E_V, and E_i are further lowered to -0.75, 0.20, and -0.28 eV, respectively, signaling the n-type semiconductor. Note that the slight difference between E_g of ML Te on TL, BL, and ML graphene arises from the blurred band-edge measured by STS, which can be attributed to the convolution of the density of states of the top layer Te and the underlying graphene.

Statistics of STS results on the ML Te films on TL, BL, and ML graphene/SiC are carried out on different samples. (The STM images and the dI/dV spectra of five more samples are shown in Figure S2, Supporting Information). As displayed in Figure 2k, the averaged values of E_i explicitly show that the ML Te on TL graphene is p-type, while it is n-type on BL or ML graphene. The charge modulation of graphene/SiC can be considered as a compromise between electron doping from SiC and the dielectric screening of graphene. The decreased thickness of graphene suppresses the screening effect and thus enhances the electron transfer from SiC to ML Te. Ristein et al.[26] estimated that the area electron density of ML graphene/SiC is 1.2×10^{13} cm^{-2}. Then the area electron density of TL graphene/SiC can be calculated as 2.4×10^{12} cm^{-2} since it is

proportional to the difference between E_V and the position of the Dirac point.[27] Considering the charge (hole) density of Te (1.5×10^{12} cm^{-2}) determined by the quantum oscillation measurements,[30] the graphene/SiC partially transfers its electrons to Te. The carrier type of Te can be reversed when the electron density of the underlying substrate is high enough (ML or BL graphene/SiC). Indeed, the enhanced electron doping effect is presented as the band lowering of Te films upon the decrease of graphene thickness.

By controlling the graphitization process of the SiC substrate, the surface covered by graphene with different thickness in different areas is obtained. And ML Te films can be grown across the graphene steps with continuous lattice, probably due to the strong covalent bonds along the helical chains. **Figure 3**a shows the 3D STM image of ML Te film covering two adjacent terraces of graphene (the original image is shown in Figure S3, Supporting Information). The film maintains continuous lattice without significant distortion across the step edge. The step height difference is about 80 pm, corresponding to the height between the ML graphene on an upper SiC terrace and TL graphene on the lower SiC terrace (see Figure 3b). Figure 3c presents the in-plane atomic configuration, in which Te chains are arranged in parallel with each other with an angle of $\approx 32°$ relative to the step edge. It is worth mentioning that different orientation angles have been observed and the electronic structures of Te films are not sensitively affected (see Supporting Information). The dI/dV spectra are measured across the step, and the color-coded map is plotted in Figure 3d. Away from the step edge, as expected, the ML Te is n-type on the ML graphene/SiC (left), while it is p-type on TL graphene/SiC (right). Near the step, a type-II band alignment is observed, indicating the formation of an in-plane p–n junction. The length of the junction region (space charge region), where the band bending occurs, is about 6.2 nm. The band bending is quantitatively measured as shown in Figure 3e, where the offset of E_V is determined as $\Delta E_V = 0.17$ eV and the offset of E_C is $= 0.34$ eV. A large build-in electrical field is further calculated to be 4×10^5 V cm^{-1}. Based on this in-plane p–n junction, the real diode transport at room temperature can be expected.

The key of the above strategy is to precisely tune the doping effect of the substrate with in-plane spatial variance, which
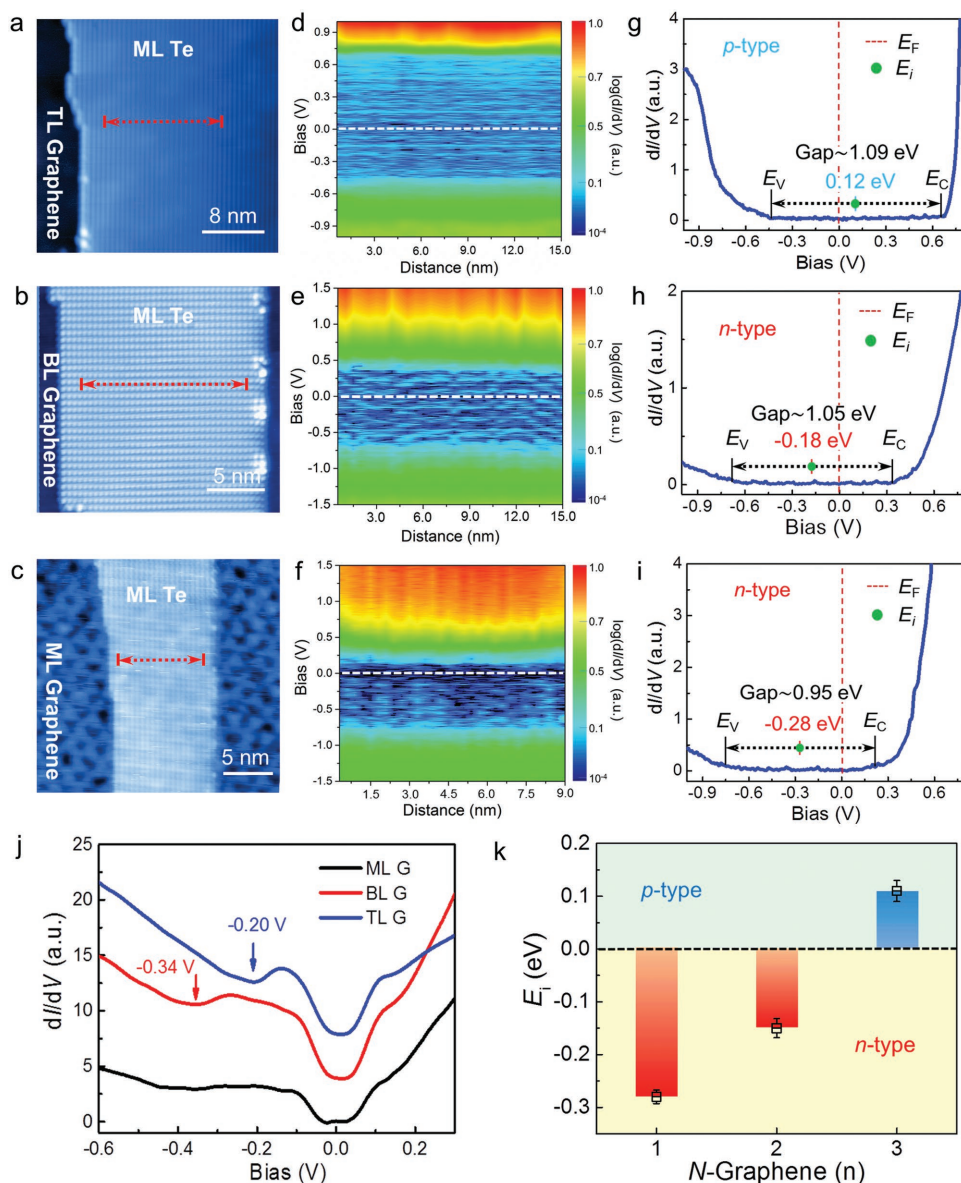
Figure 2. Tuning of the electronic structures of ML Te by the thickness of graphene on SiC. a–c) The STM images (−1.2 V/100 pA) of ML Te on TL, BL, and ML graphene/SiC. d–f) The 2D color mappings of dI/dV spectra (−1.0 V/100 pA) taken along the dashed red lines in (a–c) at an interval of 0.5 nm, respectively. The white dashed lines indicate the position of E_F. g–i) Representative dI/dV spectra of corresponding samples shown in (a–c). The green dots mark the location of E_i, while the red dashed line indicates the location of E_F. j) dI/dV spectra of TL, BL, and ML graphene/SiC substrates of the samples shown in (a–c), respectively. The spectra are shifted vertically for clarity and the arrows indicate the location of the Dirac point. k) The statistical values of E_i with respect to the thickness of graphene. Each data point is averaged over 20 independent sampling points of different samples. The columns are guides to the eye.

can be realized by the patterning of the screening layer on the donor/acceptor substrate. For example, the recent progress on the anisotropic etching of graphene[31] makes it possible to obtain designed patterns on the graphene/SiC substrate. In-plane p–n junctions are formed at the pattern edges by growing ultrathin films or transferring mechanically exfoliated 2D materials, as long as the carrier type can be reversed with feasible tuning. In most cases, the existing semiconductor lithography techniques[32,33] can be applied to fabricate field effect structures that induce the formation of p–n junctions in the overlayers. Moreover, this approach is advantageous because the electronic

materials can be free of the lithography processes—the possible contamination or thermal deterioration is avoided.

In summary, we demonstrate the realization of a 2D in-plane p–n junction with a homogeneous semiconducting monolayer Te film. The doping effect of SiC substrate is screened by the overlying graphene at different degrees depending on its thickness, which is carefully controlled. We grow monolayer Te film across the step edge between two adjacent terraces of graphene. And by using in situ scanning tunneling microscopy/spectroscopy, we directly characterize the band bending configuration of the high quality in-plane p–n junction. Toward
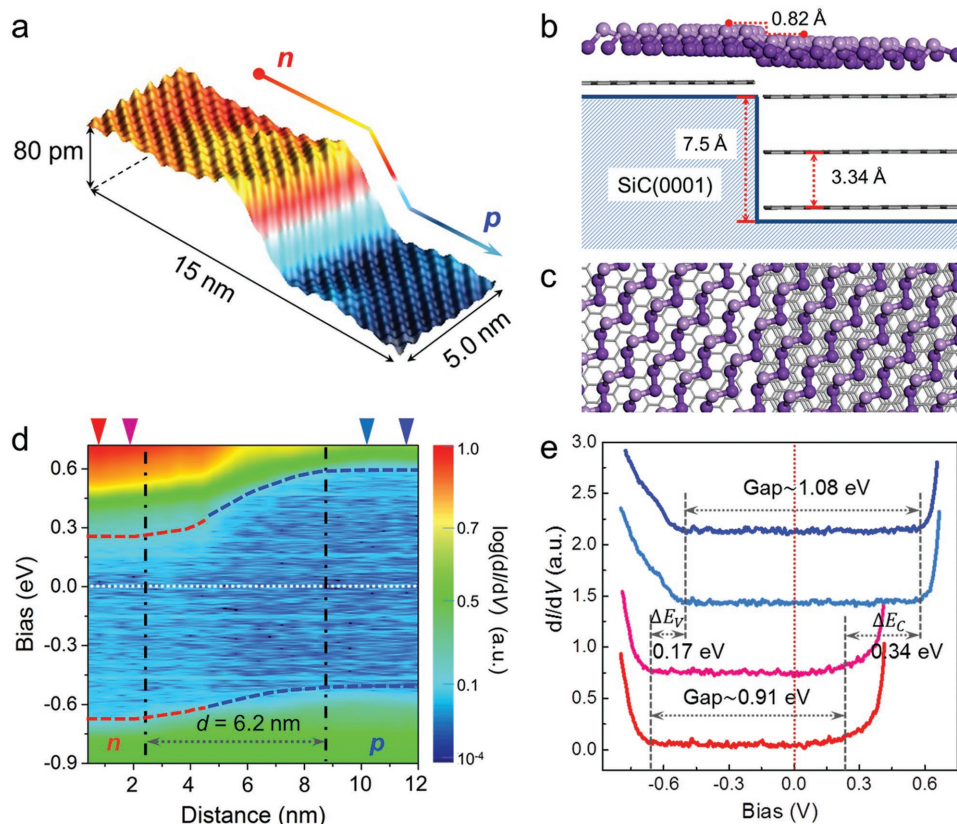
Figure 3. In-plane p–n junction of monolayer Te. a) 3D STM image (−1.0 V/100 pA) of ML Te covering two adjacent graphene terraces with continuous lattice across the step edge. b,c) Side- and top-views of the schematic of ML Te across the step between ML and TL graphene on adjacent SiC terraces. The topmost Te atoms on the surface are highlighted in pink. The step heights of 6H-SiC and graphene are 7.50 and 3.34 Å, respectively. In the current configuration that the ML graphene on the upper SiC terrace and TL graphene on the lower terrace, the step height is ≈0.82 Å. The angle between Te chains and the step edge is ≈32°, in accordance with the experimental observation. d) The 2D color mapping with logarithmic scale of dI/dV spectra (−1.0 V/100 pA) taken across the step edge with the interval of 0.5 nm. The red and the blue dashed lines label the locations of E_V and E_C, which are bending near the step edge (between the black dash-dotted lines). e) dI/dV spectra taken at the positions labeled in (d) with the corresponding colors. The curves are shifted vertically for clarity.

the practicable fabrication of electronic devices based on the in-plane p–n junctions, the reported idea can be readily extended by using other patternable templates compatible with lithography process, or mechanically exfoliated 2D flakes as the electronic materials.

Supporting Information

Supporting Information is available from the Wiley Online Library or from the author.

Acknowledgements

Conflict of Interest

The authors declare no conflict of interest.

Keywords

[1] K. S. Novoselov, A. K. Geim, S. V. Morozov, D. Jiang, M. I. Katsnelson, I. V. Grigorieva, S. V. Dubonos, A. A. Firsov, *Nature* **2005**, *438*, 197.

[2] B. Feng, Z. Ding, S. Meng, Y. Yao, X. He, P. Cheng, L. Chen, K. Wu, *Nano Lett.* **2012**, *12*, 3507.

[3] X. Wu, Y. Shao, H. Liu, Z. Feng, Y. L. Wang, J. T. Sun, C. Liu, J. O. Wang, Z. L. Liu, S. Y. Zhu, Y. Q. Wang, S. X. Du, Y. G. Shi, K. Ibrahim, H. J. Gao, *Adv. Mater.* **2017**, *29*, 1605407.

[4] X. C. Huang, J. Q. Guan, Z. J. Lin, B. Liu, S. Y. Xing, W. H. Wang, J. D. Guo, *Nano Lett.* **2017**, *17*, 4619.

[5] Y. Kubota, K. Watanabe, O. Tsuda, T. Taniguchi, *Science* **2007**, *317*, 932.

[6] B. Radisavljevic, A. Radenovic, J. Brivio, V. Giacometti, A. Kis, *Nat. Nanotechnol.* **2011**, *6*, 147.

[7] L. Li, Y. Yu, G. J. Ye, Q. Ge, X. Ou, H. Wu, D. Feng, X. H. Chen, Y. Zhang, *Nat. Nanotechnol.* **2014**, *9*, 372.

[8] G. D. Nguyen, H. Z. Tsai, A. A. Omrani, T. Marangoni, M. Wu, D. J. Rizzo, G. F. Rodgers, R. R. Cloke, R. A. Durr, Y. Sakai, F. Liou, A. S. Aikawa, J. R. Chelikowsky, S. G. Louie, F. R. Fischer, M. F. Crommie, *Nat. Nanotechnol.* **2014**, *12*, 1077.

[9] A. K. Geim, I. V. Grigorieva, *Nature* **2013**, *499*, 419.

[10] K. S. Novoselov, A. Mishchenko, A. Carvalho, A. H. Castro Neto, *Science* **2016**, *353*, aac9439.

[11] Y. Gong, J. Lin, X. Wang, G. Shi, S. Lei, Z. Lin, X. Zou, G. Ye, R. Vajtai, B. I. Yakobson, H. Terrones, M. Terrones, B. K. Tay, J. Lou, S. T. Pantelides, Z. Liu, W. Zhou, P. M. Ajayan, *Nat. Mater.* **2014**, *13*, 1135.

[12] Z. W. Zhang, P. Chen, X. D. Duan, K. T. Zang, J. Lou, X. F. Duan, *Science* **2017**, *357*, 788.

[13] Y. Q. Wang, X. Wu, Y. L. Wang, Y. Shao, T. Lei, J. O. Wang, S. Y. Zhu, H. Guo, L. X. Zhao, G. F. Chen, S. Nie, H. M. Weng, K. Ibrahim, X. Dai, Z. Fang, H. J. Gao, *Adv. Mater.* **2016**, *28*, 5013.

[14] J. M. Cai, C. A. Pignedoli, L. Talirz, P. Ruffieux, H. Söde, L. Liang, V. Meunier, R. Berger, R. Li, X. Feng, K. Müllen, R. Fasel, *Nat. Nanotechnol.* **2014**, *9*, 896.

[15] P. K. Sahoo, S. Memaran, Y. Xin, L. Balicas, H. R. Gutiérrez, *Nature* **2018**, *553*, 63.

[16] D. L. Duong, S. J. Yun, Y. H. Lee, *ACS Nano* **2017**, *11*, 11803.

[17] C. Huang, S. Wu, A. M. Sanchez, J. J. P. Peter, R. Beanland, J. S. Ross, P. Rivera, W. Yao, D. H. Cobden, X. Xu, *Nat. Mater.* **2014**, *13*, 1096.

[18] S. H. Kim, K. H. Jin, B. W. Kho, B. G. Park, F. Liu, J. S. Kim, H. W. Yeom, *ACS Nano* **2017**, *11*, 9671.

[19] M. Y. Li, Y. Shi, C. C. Cheng, L. S. Lu, Y. C. Lin, H. L. Tang, M. L. Tsai, C. W. Chu, K. H. Wei, J. H. He, W. H. Chang, K. Suena a, L. J. Li, *Science* **2015**, *349*, 524.

[20] M. Rösner, C. Steinke, M. Lorke, C. Gies, F. Jahnke, T. O. Wehling, *Nano Lett.* **2016**, *16*, 2322.

[21] J. J. Zhao, K. Cheng, N. N. Han, J. F. Zhang, *WIREs Comput. Mol. Sci.* **2018**, *8*, e1353.

[22] J. F. Zhang, W. Y. Xie, J. J. Zhao, S. B. Zhang, *2D Mater.* **2017**, *4*, 015038.

[23] Y. Jiang, Y. Y. Sun, M. Chen, Y. Wang, Z. Li, C. Song, K. He, L. Wang, X. Chen, Q. K. Xue, X. Ma, S. B. Zhang, *Phys. Rev. Lett.* **2012**, *108*, 066809.

[24] Y. L. Wang, J. Ren, C. L. Song, Y. P. Jiang, L. L. Wang, K. He, X. Chen, J. F. Jia, S. Meng, E. Kaxiras, Q. H. Xue, X. C. Ma, *Phys. Rev. B* **2010**, *82*, 245420.

[25] C. Berger, Z. Song, T. Li, X. Li, A. Y. Ogbazghi, R. Feng, Z. Dai, A. N. Marchenkov, E. H. Conrad, P. N. First, W. A. de Heer, *J. Phys. Chem. B* **2004**, *108*, 19912.

[26] J. Ristein, S. Mammadov, T. Seyller, *Phys. Rev. Lett.* **2012**, *108*, 246104.

[27] E. Moreau, S. Godey, X. Wallart, I. Razado-Colambo, J. Avila, M.-C. Asensio, D. Vignaud, *Phys. Rev. B* **2013**, *88*, 075406.

[28] Q. Wang, W. Zhang, L. Wang, K. He, X. Ma, Q. Xue, *J. Phys.: Condens. Matter* **2013**, *25*, 095002.

[29] P. Lauffer, K. V. Emtsev, R. Graupner, T. Seyller, L. Ley, *Phys. Rev. B* **2008**, *77*, 155426.

[30] K. Klitzing, G. Landwehr, *Solid State Commun.* **1971**, *9*, 2201.

[31] Z. W. Shi, R. Yang, L. C. Zhang, Y. Wang, D. H. Liu, D. X. Shi, E. G. Wang, G. Y. Zhang, *Adv. Mater.* **2011**, *23*, 3061.

[32] J. Gierak, *Semicond. Sci. Technol.* **2009**, *24*, 23.

[33] M. Henini, *III–Vs Rev.* **1999**, *12*, 18.

1802065 (5 of 5)